Trapping of Oxygen Vacancies at Crystallographic Shear Planes in Acceptor-Doped Pb-Based Ferroelectrics

*Dmitry Batuk, Maria Batuk, Alexander A. Tsirlin, Joke Hadermann and Artem M. Abakumov**

Abstract: *We report on defect chemistry of the acceptor Fe^{3+} doping in ferroelectric $PbTiO_3$. With advanced transmission electron microscopy, powder X-ray and neutron diffraction we demonstrate that even at concentrations as low as ~1.7% (~$ABO_{2.95}$), the oxygen vacancies are trapped into extended planar defects, crystallographic shear planes. We investigate the evolution of these defects upon doping and unravel their detailed atomic structure using the formalism of superspace crystallography, thus unveiling their role in non-stoichiometry in the Pb-based perovskites.*

Perovskite-based ferroelectrics are widely applied in modern technologies because their dielectric properties can be tuned by appropriate doping.[1] Doping of $Pb[Zr_xTi_{1-x}]O_3$ with acceptors (B-cations with oxidation state lower than +4) causes "hardening" of the material, making it suitable for actuators or resonators. It implies a pinched hysteresis loop, decreasing dielectric losses and bulk resistivity. Owing to the technological importance of doping, its microscopic mechanism is actively studied both experimentally and theoretically. Replacement of Ti^{4+} or Zr^{4+} by acceptor cations introduces oxygen vacancies, which form a defect associate with an acceptor atom. When few at. % Fe^{3+} are doped into the $PbTiO_3$ or $Pb[Zr_xTi_{1-x}]O_3$ ceramics, the defect associate can be written using the Kröger-Vink notations as $(Fe'_{Ti} - V_O^{\cdot\cdot})^{\cdot}$ (the prime and dot denote the charges of -1 and +1, respectively).[2–6] Since the overall charge of the defect associate is +1, negatively charged lead vacancies V''_{Pb} are required for the charge compensation, and therefore lead deficiency is assumed.[4] The segregation of oxygen vacancies becomes particularly important in the context of Scott and Dawber's conjecture on the oxygen-vacancy ordering as a polarization fatigue mechanism in perovskite ferroelectrics.[7] Polarization fatigue, the degradation of remnant polarization upon repetitive switching, is related in this model to electromigration of randomly distributed oxygen vacancies and their ordering into planar arrays pinning ferroelectric domain wall motion.[8] The behavior of diluted oxygen vacancies is usually weakly correlated, and the oxygen-vacancy-based fatigue mechanism assumes that they interact only above a certain concentration limit, which is estimated at ~7% ($ABO_{2.80}$). The exact ordering pattern of point oxygen vacancies is not yet clear and their role in the polarization fatigue is still under debate.[9–11] In this contribution, we report on the peculiarities of defect chemistry of the acceptor Fe^{3+} doping in ferroelectric $PbTiO_3$. We demonstrate that even at a vacancy concentration as low as ~1.7% (~$ABO_{2.95}$) the oxygen vacancies are trapped into extended planar defects, namely crystallographic shear (CS) planes. Although the formation of CS planes in ferroelectric perovskites was put forward 40 years ago, neither their direct experimental observation nor their structure have been reported.[12] Here, we investigate the evolution of these planar defects upon doping, unravel their atomic structure and explain their possible role in the Pb and O deficiency in the acceptor-doped Pb-based ferroelectrics.

The $Pb_{1-x}(Ti_{1-z}Fe_z)_{1+x}O_{3-y}$ ($0 \le z \le 1$) materials were prepared by a solid state reaction at 860-1100°C, with the annealing temperature rising concomitantly with the Ti content (see details in the Experimental section and Tables S1-S2 of Supporting Information (SI)). X-ray powder diffraction (XPD) patterns of the $Pb_{1-x}(Ti_{1-z}Fe_z)_{1+x}O_{3-y}$ ($0 \le z \le 1$) series (Fig. S1-S3 of SI) demonstrate systematic changes with increasing Fe^{3+} content: the tetragonal distortion of the perovskite unit cell diminishes and progressive anisotropic reflection broadening occurs for z up to 0.15, followed by reflection splitting and the appearance of extra peaks above z = 0.2. This behavior is indicative of extended defects that form an ordered pattern at higher z. The high angle annular dark field scanning transmission electron microscopy (HAADF-STEM) images of the milestone compounds in the $Pb_{1-x}(Ti_{1-z}Fe_z)_{1+x}O_{3-y}$ system are shown in Fig. 1. The eye-catching feature of the images is the arrangement of the bright dots corresponding to the Pb atomic columns (Z_{Pb} = 82): they form a perovskite square pattern, which is separated into domains by the planar defects. The dots corresponding to the Ti/Fe-O columns are weaker (Z_{Ti} = 22, Z_{Fe} = 26, Z_O = 8). At low Fe^{3+} concentration (z = 0.1), the defects occur randomly in the perovskite matrix, but are confined to the $(101)_p$ or $(10\bar{1})_p$ perovskite planes. At z = 0.2, the defects demonstrate correlated behavior: they tend to align parallel to the $(101)_p$ plane equidistantly spaced by ~60 Å. Owing to weak interactions between defects, their orientation and interplanar spacing vary locally and result in a wavy appearance. Further increase of the Fe^{3+} content up to z ~ 0.975 introduces regular long range order of the planar defects. The thickness of the perovskite blocks between the defect planes decreases with z and the orientation of the defect planes changes gradually from $(101)_p$ towards $(70\underline{1}1)_p$. Finally, at high Fe^{3+} content (~0.975 < z ≤ 1) the materials form "$Pb_2Fe_2O_5$"-type highly defective structures.[13–15]

[*] Dr. D. Batuk, Dr. M. Batuk, Prof. Dr. J. Hadermann, Dr. A. M. Abakumov
EMAT, University of Antwerp, Groenenborgerlaan 171, 2020, Antwerp (Belgium)
E-mail: artem.abakumov@uantwerpen.be

Dr. A. M. Abakumov
Chemistry Department, Moscow State University, 119991, Moscow (Russia)

Dr. A. A. Tsirlin
National Institute of Chemical Physics and Biophysics, 12618, Tallinn (Estonia); Experimental Physics VI, EKM, University of Augsburg, 86159 Augsburg (Germany)

Supporting Information for this article is available on the WWW under http://…

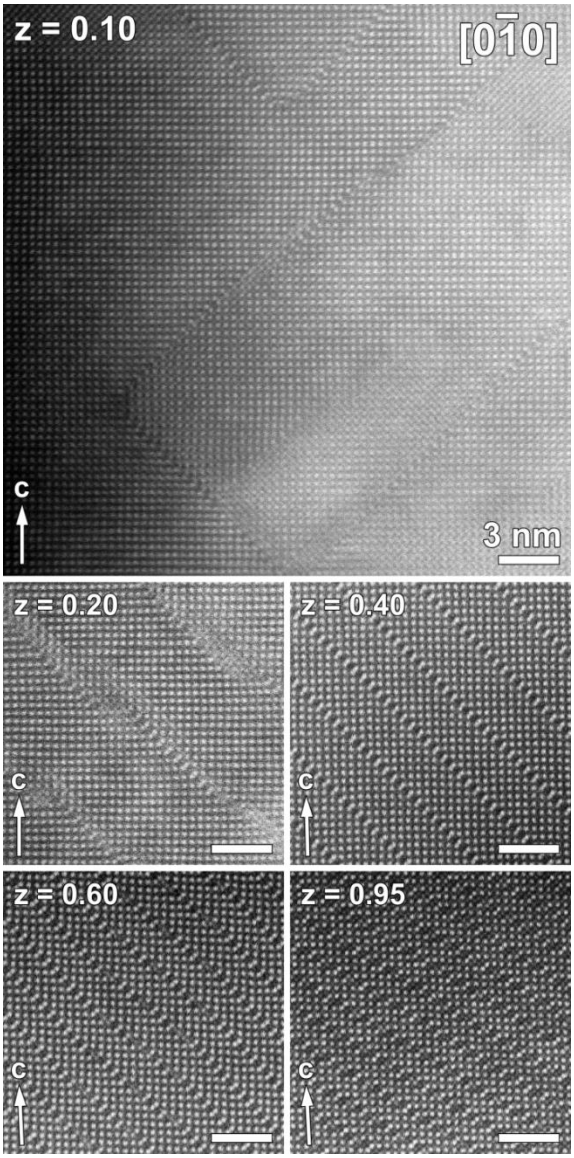

Figure 1. HAADF-STEM images of selected $Pb_{1-x}(Ti_{1-z}Fe_z)_{1+x}O_{3-y}$ materials. The orientation of the defect planes is ~$(101)_p$ and ~$(10\bar{1})_p$ for z = 0.10; $(101)_p$ for z = 0.20, 0.40; (10011) for z = 0.60; $(7011)_p$ for z = 0.95.

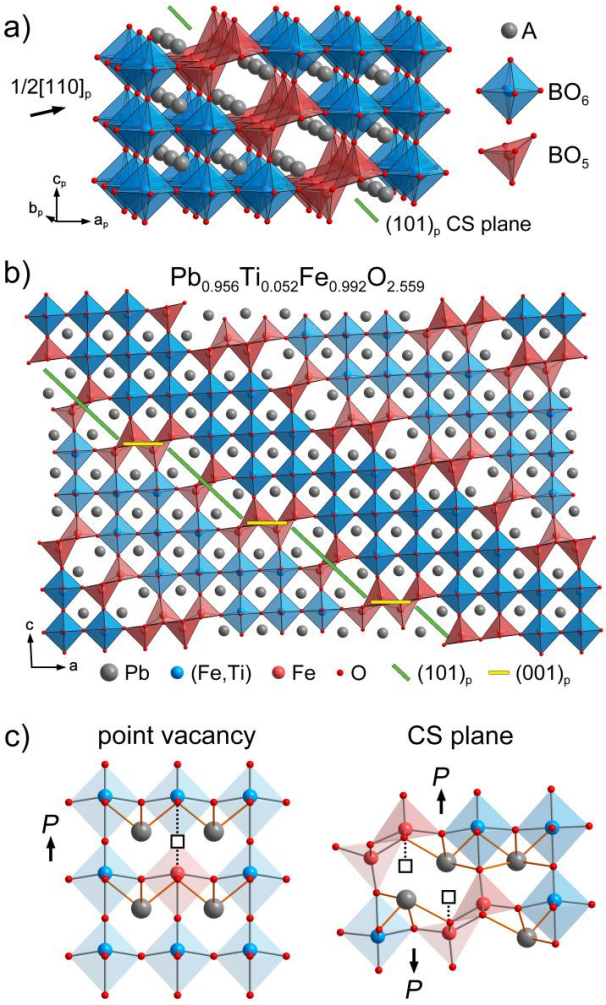

Figure 2. (a) Schematic drawing of the $(101)_p$ CS plane in perovskite. (b) A representative 13*a*×1*b*×8*c* fragment of the z = 0.95 refined structure. (c) Comparison between two models of the Fe^{3+} doping in $PbTiO_3$: defect associate $(Fe'_{Ti} - V_O^{\cdot})^{\cdot}$ formed by oxygen vacancy (square) and the Fe^{3+} cation in incomplete FeO_5 polyhedron (red), in accordance with refs. [6,19] and Fe^{3+} segregation at the CS plane.

These planar defects can be identified as CS planes (compare the images in Fig. 1 to those of perovskites CS structures in refs. [16–18]). An $(h0l)_p$ CS plane is formed by a displacement of one part of the ABO_3 perovskite structure with respect to another over a vector $½[110]_p$. The displacement transforms corner-sharing BO_6 octahedra along the plane into edge-sharing BO_5 tetragonal pyramids (Figure 2a). This reduces the oxygen content by trapping anion vacancies at the CS plane and changing the connectivity of the metal-oxygen polyhedra. The shear operation creates infinite tunnels filled by double A-cation columns.[13] These A positions demonstrate a highly asymmetric oxygen environment and can only be occupied by stereochemically active lone pair cations, such as Pb^{2+} and Bi^{3+}. For that reason, the oxygen accumulation in CS planes cannot be envisaged in ferroelectrics like $BaTiO_3$, where only alkali or alkali-earth metals are present in the A position.

The interpretation of the planar defects as CS planes is directly confirmed by the Rietveld refinement of the well-ordered z = 0.95 crystal structure against neutron powder diffraction (NPD) data. Due to the large relaxation at the CS planes, the structure is incommensurately modulated. We described the structure using a (3+1)D structural model developed earlier for the $(Pb,Bi)_{1-x}Fe_{1-x}O_{3-y}$ system (Table S4 of SI).[16,18] The model could also be applied to other members of the $Pb_{1-x}(Ti_{1-z}Fe_z)_{1+x}O_{3-y}$ family allowing interpretation of their XPD data. The corresponding crystallographic parameters are summarized in Table S3 of SI. The z = 0.95 compound is antiferromagnetically (AFM) ordered at room temperature. To avoid the magnetic contribution, the refinement was performed using the NPD data at *T* = 900 K (Tables S4-S5 and Fig. S4-S5 of SI). A representative 13*a*×1*b*×8*c* fragment of the z = 0.95 structure is shown in Fig. 2b. The CS planes in this material adopt an orientation close to $(7011)_p$. Generally, the $(h0l)_p$ CS plane can be considered as an ordered sequence of alternating $(001)_p$ and

$(101)_p$ segments. The segments of both types contain chains of distorted FeO_5 square pyramids sharing common basal edges. The $(101)_p$ and $(001)_p$ segments are based on double and quadruple pyramidal chains, respectively. The $(101)_p$ segments reduce the oxygen content, while the $(001)_p$ segments reduce the Pb/(Fe,Ti) ratio. The $(h0l)_p$ orientation of the planes is related to the components of the modulation vector as $h/l = \alpha/\gamma$. Based on the structural model, the chemical composition can be expressed as $Pb_{1+\alpha-\gamma}(Ti_{1-z}Fe_z)_{1-\alpha+\gamma}O_{3-\alpha-3\gamma}$. In the Pb-Ti-Fe-O system, the orientation of the CS planes is primarily governed by the Fe/Ti ratio, whereas the oxygen content defines the Pb deficiency.

Spatially resolved electron energy loss spectroscopy (EELS) and energy dispersive X-ray spectroscopy (EDX) demonstrate that the BO_5 tetragonal pyramids at the CS planes are occupied exclusively by the Fe^{3+} cations (Fig. 3 and Fig. S6 of SI). The Fe^{3+} cations segregate along the CS planes together with the oxygen vacancies, whereas the Ti^{4+} cations are located in the perovskite blocks. One could argue that this segregation tendency might be a mere consequence of insufficient homogenization of the Fe^{3+} dopants. In order to refute this scenario, we prepared the $Pb_{1-x}(Ti_{1-z}Fe_z)_{1+x}O_{3-y}$ samples using chemical homogenization. The HAADF-STEM images of the z = 0.05 (1.7% of oxygen vacancies) and z = 0.3 samples (9.9% of oxygen vacancies) (Fig. S7-S8 of SI) clearly demonstrate the presence of the CS planes, reflecting that their formation is intrinsic to this system.

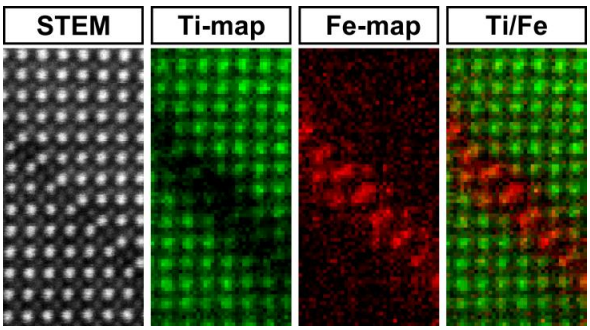

Figure 3. High resolution STEM-EELS elemental maps of the z = 0.2 sample showing the Fe^{3+} segregation at the CS plane.

The local Fe-O atomic arrangement at the CS planes resembles the geometry of the $(Fe'_{Ti} - V_O^{\cdot\cdot})^{\cdot}$ polar defect associate (Fig. 2c).[20] Thus, the formation of the CS planes can be considered as their condensation. In contrast to the single $(Fe'_{Ti} - V_O^{\cdot\cdot})^{\cdot}$ associate with the dipole moment directed along the bulk polarization of the crystal, at the CS plane the associates condense "tail-to-tail", so that their dipoles are aligned antiparallel along the *c*-axis on either side of the CS plane. The off-center displacements of the Pb and Ti cations in the perovskite blocks also occur along the *c*-axis with the maximum amplitudes near the CS planes and opposite orientation on both sides of the perovskite blocks, whereas at the center of the perovskite blocks the displacements are absent. We can consider a single CS plane in the perovskite matrix acting as a 180° pinned ferroelectric domain wall. Thus, an ordered array of CS planes results in an antipolar structure.[6,19] It is also noteworthy noting that the condensation of the defect associates might be sensitive to the preparation conditions. The XPD patterns of the $PbTi_{1-z}Fe_zO_{3-\delta}$ solid solutions prepared using wet chemistry at 700°C do not demonstrate the reflection splitting expected for the CS structure at least up to z = 0.5, but raising the annealing temperature to 850°C and 1000°C produces XPD patterns characteristic of CS planes.[21]

At high doping levels, Fe^{3+}-doped $PbTiO_3$ develops AFM order, which is seen in the room-temperature NPD pattern of the *z* = 0.95 sample (Fig. S9 of SI). Temperature dependence of the magnetic susceptibility for the *z* = 0.9 sample indicates an AFM transition with the Néel temperature of T_N = 485 K (Fig. 4). By contrast, the *z* = 0.3 sample demonstrates an overall paramagnetic behavior, but its inverse magnetic susceptibilities follows the Curie-Weiss law above 400 K only, and the Curie-Weiss temperature θ is as high as 400 K (Fig. 4). At $T < \theta$, exchange interactions between the Fe^{3+} ions segregated at the CS planes may induce short-range magnetic order that results in deviations from the paramagnetic Curie-Weiss behavior. However, no long-range magnetic order is formed.

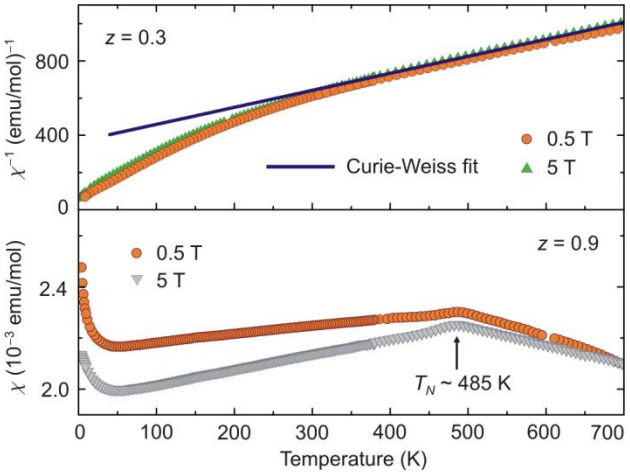

Figure 4. Top panel: inverse magnetic susceptibility of the *z* = 0.3 sample and the Curie-Weiss fit above 400 K with the paramagnetic effective moment of 2.96 μ_B (26% of Fe^{3+} ions) and the AFM Curie-Weiss temperature θ = 400 K. Bottom panel: magnetic susceptibility of the *z* = 0.9 sample revealing an AFM ordering transition at T_N ~ 485 K. The weak field dependence may be due to trace amounts of a ferrimagnetic impurity, such as $PbFe_{12}O_{19}$ or Fe_2O_3.

To summarize, the substitution of Ti^{4+} by Fe^{3+} in $PbTiO_3$ leads to a condensation of the $(Fe'_{Ti} - V_O^{\cdot\cdot})^{\cdot}$ defect associates into CS planes already at an oxygen vacancy concentration as low as ~1.7%. The CS planes occur as random defects at low Fe^{3+} doping, and demonstrate well-established long range order at the Fe^{3+} content ≥ 20 at.%. The structure of the CS planes elucidates the microscopic mechanism behind the oxygen and lead deficiency in acceptor-doped Pb-based ferroelectrics. Due to the "tail-to-tail" condensation of the $(Fe'_{Ti} - V_O^{\cdot\cdot})^{\cdot}$ defect associates, a single CS plane acts as immobilized ferroelectric domain wall and their ordered arrangement renders the structure antipolar. This direct information on the defect chemistry of perovskite ferroelectrics opens broad perspectives for experimental and theoretical studies of extended defects and their influence on the dielectric performance of these materials.

Experimental Section

The solid-state synthesis was performed from PbO (Sigma-Aldrich, ≥ 99.9%), Fe_2O_3 (Sigma-Aldrich, ≥ 99.98%), and TiO_2 anatase (Aldrich, ≥ 99.8%). The oxides were ground, pelletized and annealed with intermediate regrindings at the conditions summarized in Table S1 of Supporting Information. To compensate for the lead oxide volatility, ~5 wt.% PbO were added on the annealing step next to the last one. First, the $Pb(Ti_{1-z}Fe_z)O_{3-y}$ samples were prepared. After identifying their actual compositions (Table S2 of Supporting Information), the single phase $Pb_{1-x}(Ti_{1-z}Fe_z)_{1+x}O_{3-y}$ samples were produced. The soft-chemistry procedure was similar to that reported in ref. [21], the details are given in Supporting Information.

The XPD patterns were acquired on a Huber G670 diffractometer (Cu $K_{\alpha 1}$ radiation). The NPD data were collected on the HRPT diffractometer at the Laboratory for Neutron Scattering of Paul Scherrer Institute (LNS PSI, Villigen, Switzerland) at wavelength 1.8857 Å in the 2θ range 8-160° in a 8 mm vanadium container at 900 K. Crystal structure analysis was performed with JANA 2006.[22]

The TEM samples were prepared by crushing the powder in ethanol and depositing the suspension on TEM holey carbon grids. HAADF-STEM images, STEM-EDX and STEM-EELS maps were acquired on a FEI-Tecnai G2 microscope and aberration-corrected FEI Titan^3 60-300 microscope equipped with a Super-X detector. The STEM-EDX and STEM-EELS data were recorded at 200 kV and 120 kV, respectively, with a convergence semi-angle of 21 mrad (probe size of about 1 Å).

Magnetic susceptibility was measured using the vibrating sample magnetometer (VSM) insert of Quantum Design PPMS. Measurements above 400 K were performed using the oven setup in high vacuum (10^{-5} torr).

Acknowledgements

A.M.A. is grateful to the Russian Science Foundation (grant 14-13-00680). AT was funded by the Mobilitas grant MTT77 of the ESF and by the Federal Ministry for Education and Research through the Sofja Kovalevskaya Award of Alexander von Humboldt Foundation.

Keywords: transmission electron microscopy; perovskite ferroelectrics; acceptor doping; oxygen vacancy; planar defects

[1] B. Jaffe, W. R. Cook, H. Jaffe, *Piezoelectric Ceramics*, Academic Press, London, **1971**.

[2] T. R. N. Kutty, R. Balachandran, *Mater. Chem. Phys.* **1985**, *13*, 467–475.

[3] D. J. Keeble, M. Loyo-Menoyo, Z. I. Y. Booq, R. R. Garipov, V. V. Eremkin, V. Smotrakov, *Phys. Rev. B.* **2009**, *80*, 1–7.

[4] R. A. Eichel, *J. Electroceramics* **2007**, *19*, 9–21.

[5] H. Meštrić, R. A. Eichel, K. P. Dinse, A. Ozarowski, J. Van Tol, L. C. Brunel, *J. Appl. Phys.* **2004**, *96*, 7440–7444.

[6] A. Chandrasekaran, D. Damjanovic, N. Setter, N. Marzari, *Phys. Rev. B.* **2013**, *88*, 1–7.

[7] J. F. Scott, M. Dawber, *Appl. Phys. Lett.* **2000**, *76*, 3801–3803.

[8] M. Dawber, J. F. Scott, *Appl. Phys. Lett.* **2000**, *76*, 1060–1062.

[9] X. J. Lou, *J. Appl. Phys.* **2009**, *105*, 024101.

[10] M. Dawber, K. M. Rabe, J. F. Scott, *Rev. Mod. Phys.* **2005**, *77*, 1083–1130.

[11] A. K. Tagantsev, I. Stolichnov, E. L. Colla, N. Setter, *J. Appl. Phys.* **2001**, *90*, 1387–1402.

[12] A. H. Meitzler, *Ferroelectrics* **1976**, *11*, 503–510.

[13] A. M. Abakumov, J. Hadermann, S. Bals, I. V. Nikolaev, E. V. Antipov, G. Van Tendeloo, *Angew. Chem.* **2006**, *45*, 6697–6700.

[14] A. M. Abakumov, J. Hadermann, G. Van Tendeloo, E. V. Antipov, *J. Am. Ceram. Soc.* **2008**, *91*, 1807–1813.

[15] J. Hadermann, A. M. Abakumov, I. V. Nikolaev, E. V. Antipov, G. Van Tendeloo, *Solid State Sci.* **2008**, *10*, 382–389.

[16] A. M. Abakumov, D. Batuk, J. Hadermann, M. G. Rozova, D. V. Sheptyakov, A. A. Tsirlin, D. Niermann, F. Waschkowski, J. Hemberger, G. Van Tendeloo, *Chem. Mater.* **2011**, *23*, 255–265.

[17] D. Batuk, M. Batuk, A. M. Abakumov, A. A. Tsirlin, C. McCammon, L. Dubrovinsky, J. Hadermann, *Inorg. Chem.* **2013**, *52*, 10009–10020.

[18] D. Batuk, M. Batuk, A. M. Abakumov, J. Hadermann, *Acta Crystallogr.B.* **2015**, *B71*, 127–143.

[19] H. Meštrić, R. A. Eichel, T. Kloss, K. P. Dinse, S. Laubach, S. Laubach, P. C. Schmidt, K. A. Schönau, M. Knapp, H. Ehrenberg, *Phys. Rev. B.* **2005**, *71*, 1–10.

[20] P. Erhart, R. A. Eichel, P. Träskelin, K. Albe, *Phys. Rev. B.* **2007**, *76*, 1–12.

[21] H. Ganegoda, J. A. Kaduk, C. U. Segre, *Powder Diffr.* **2013**, *28*, 238–245.

[22] V. Petříček, M. Dušek, L. Palatinus, *Zeitschrift für Krist.* **2014**, *229*, 345–352.

Entry for the Table of Contents

COMMUNICATION

In ferroelectric $PbTiO_3$, the substitution of Ti^{4+} by Fe^{3+} leads to a segregation of the point oxygen vacancies into crystallographic shear (CS) planes from a vacancy concentration of ~1.7% onward. The CS planes occur as random planar defects at low Fe^{3+} doping, and demonstrate long-range order when the Fe^{3+} content rises above ~20 at.%. The structure of the CS planes provides a natural mechanism for the realization of oxygen deficiency in acceptor-doped Pb-based ferroelectrics.

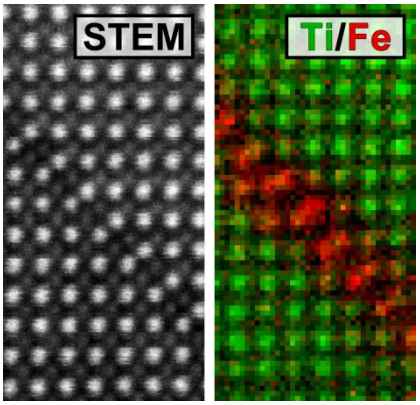

*Dmitry Batuk, Maria Batuk, Alexander A. Tsirlin, Joke Hadermann and Artem M. Abakumov**

Page No. – Page No.

Trapping of Oxygen Vacancies at Crystallographic Shear Planes in Acceptor-Doped Pb-Based Ferroelectrics